Sensors International 3 (2022) 100179

Contents lists available at ScienceDirect

Sensors International

journal homepage: www.keaipublishing.com/en/journals/sensors-international

# Machine learning algorithms based advanced optimization of EDM parameters: An experimental investigation into shape memory alloys

Ranjit Singh *, Ravi Pratap Singh, Rajeev Trehan

*Department of Industrial & Production Engineering, Dr B R Ambedkar National Institute of Technology, Jalandhar, Punjab, India*

ARTICLE INFO

*Keywords:*
Shape memory alloy
EDM
Machine learning
Optimization
GA
TLBO

ABSTRACT

In the era of advancement and progressive fourth industrial revolution culture, the demand of advanced and smart engineering materials has been increased. In this way, shape memory alloys are an excellent choice for industrial applications such as orthopedic implacers, actuators, micro-tools, fitting and screening elements, aircraft component components, military instruments, fabricating elements, and bio-medical devices, among others. This paper has been aimed to attempt the machine learning (ML) algorithms-based optimization of the different process inputs in electrical discharge machining of Cu-based shape memory alloy. The current study focused on study the behavior of response parameters along with the variation in machining input parameters The considered process input factors are namely as; pulse on time (Ton), pulse off time (Toff), peak current (Ip), and gap voltage (GV) and their effects were studied on dimensional deviation (DD) and tool wear rate (TWR). The central composite design matrix has been employed for planning the main runs. The 2-D and 3-D graphs represents the behavior of the response parameters along with variations in the machining inputs. The novelty of the work is machining of Cu-based Shape Memory Alloy (SMA) in EDM operations and optimization of parameters using Machine Learning techniques. Furthermore, machine learning based, single and multi-objective optimization of investigated responses were conducted using the desirability approach, Genetic Algorithm (GA) and Teacher Learning based Optimization (TLBO) techniques. The parametric combination attained for optimization of multiple responses (TWR and DD) is: Ton = 90.10 μs, Toff = 149.69 μs, Ip = 24.59 A & GV = 60 V; Ton = 255 μs, Toff = 15 μs, Ip = 50 A & GV = 15 V; Ton = 255 μs, Toff = 15 μs, Ip = 50 A & GV = 15 V, using desirability approach, GA method and TLBO method, respectively.

## 1. Introduction

Smart materials are in high demand in today's technologically advanced world due to their remarkable properties and applications in a broad variety of fields, from bio-medical care to manufacturing. These materials' major properties drive technology toward intelligent, differentiated, and adaptive systems that need the use of microcontrollers, sensors, and actuators. Shape Memory Alloys (SMAs) are an essential kind of shape memory material (SMM) that can keep its original shape following temperature and magnetic changes [1]. The shape memory effect (SME) is the name given to this kind of behavior. The materials also exhibit super elasticity (in metals) and visco-elasticity (in polymers) under certain circumstances [2]. The polymeric dental material created by Vernon in 1941 was termed "shape memory" after its inventor, Arne Olander, used the phrase "smart alloy" to describe a related discovery from 1932 [3]. A number of different SMAs have been created in solid, film, and even foam forms [4]. Three types of alloys have been reported: NiTi, Cu, and Fe-based [5]. In commercial sectors include consumer goods, industrial uses, constructions [6], and composites [7], as well as the automotive [8], aerospace [9], and MEMS sectors [10], the robotics [11] and even medical and fashion industries [12], the need for SMAs has increased. However, each kind of shape memory material, on the other hand, offers a unique benefit for certain needs or applications. Alidoosti et al. [13] employed a comprehensive factorial design to investigate the electrical discharge machining features of a nickel–titanium shape

* Corresponding author.
*E-mail address:* ranjitsingh.tmk@gmail.com (R. Singh).

Production and hosting by Elsevier

https://doi.org/10.1016/j.sintl.2022.100179
Received 1 March 2022; Received in revised form 1 May 2022; Accepted 3 May 2022
Available online 20 May 2022

**Nomenclature:**

| | |
|---|---|
| Ton | Pulse on time |
| Toff | Pulse off time |
| Ip | Peak current |
| GV | Gap voltage |
| DD | Dimensional Deviation |
| TWR | Tool wear rate |
| ESCM | Electric Spark cut machining |
| SMM | Shape memory material |
| EDS | Energy dispersive X-ray spectroscopy |
| CCD | Central composite design |
| RSM | Response surface methodology |
| SMA | Shape Memory Alloy |
| ML | Machine Learning |

memory alloy. The mean analysis demonstrated that the rate of NiTi material removal in the electric discharge machine process was closely related to the electro discharge energy, including the pulse current and pulse duration [14–17]. Abidi et al. [18] employed a multi-objective evolutionary algorithm (MOGA-II). According to the findings, capacitance and electrode material are the most important parameters influencing the micro EDM process. At low to moderate capacitance and low discharge voltage values, good quality micro-holes with minimal tool wear rates were found with regard to the tungsten electrode. Brass electrode, on the other hand, demonstrated a high material removal rate at the price of tool wear and micro-hole quality. When milling NiTi alloy, Gaikwad et al. [19] focused on improving electric discharge machining process parameters to enhance material removal rate. Material removal rate rises with increasing current, surface roughness increases with increasing voltage and current, and white layer thickness grows with increasing voltage. Voltage and current are the two most important elements influencing surface roughness. The best process parameters for reducing surface roughness are voltage 40 V, current 4A, pulse on 40 μs, and pulse off 9 μs. Gaikwad et al. [20] investigated and improved process parameters in NiTi 60 Electrical Discharge Machining (EDM). Daneshmand et al. [21] wanted to look into the effects of electro-discharge machining parameters like voltage and discharge current, as well as the length of time between each pulse on and off time, the rate of material removal, tool wear, relative electrode wear, and surface roughness of NiTi alloy. With an increase in pulse on time of up to 50s, tool wear rate rises, and beyond that point, tool wear decreases. Increased pulse off time reduces tool wear and MRR. The increased voltage causes a rise in MRR and TWR, as well as the growth of surface pits, lowering the quality of the machined surface.

Traditional machining of shape memory alloys is difficult due to their high ductility, severe hardening, high toughness, viscosity, and hyperelastic behavior. Because of these characteristics, complex geometries and precise measurements are difficult to obtain using typical machining processes. Shape memory alloys have several uses in fields such as aerospace, healthcare, robotics, and construction. Because they include complex curvatures, geometries, tiny holes, and so on, the items made by producing these alloys need great attention and precision dimensioning. EDM is an unconventional machining technology that can create complex geometries, micro-holes, and cavities [22]. Electric spark cut machining is a thermal technology that uses controlled pulsed releases to treat

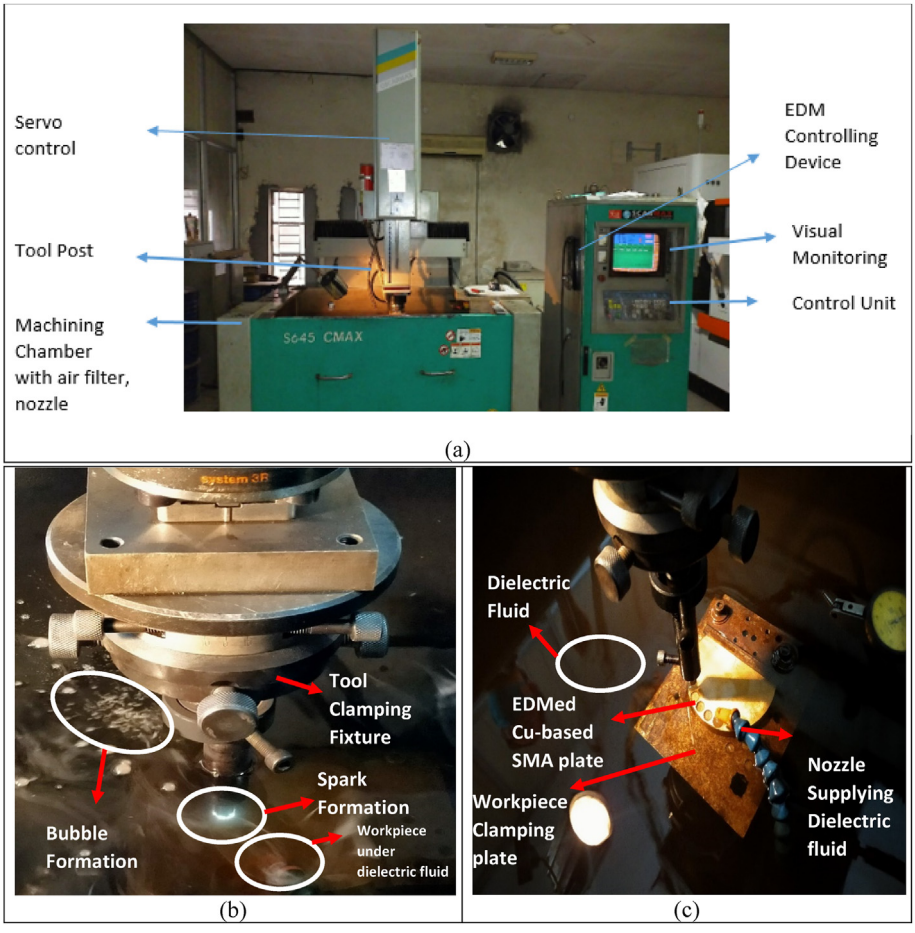


**Fig. 1.** (a) Illustration of CNC EDM set-up (b) Enlarged view of machining zone (c) EDMed Cu-based SMA.

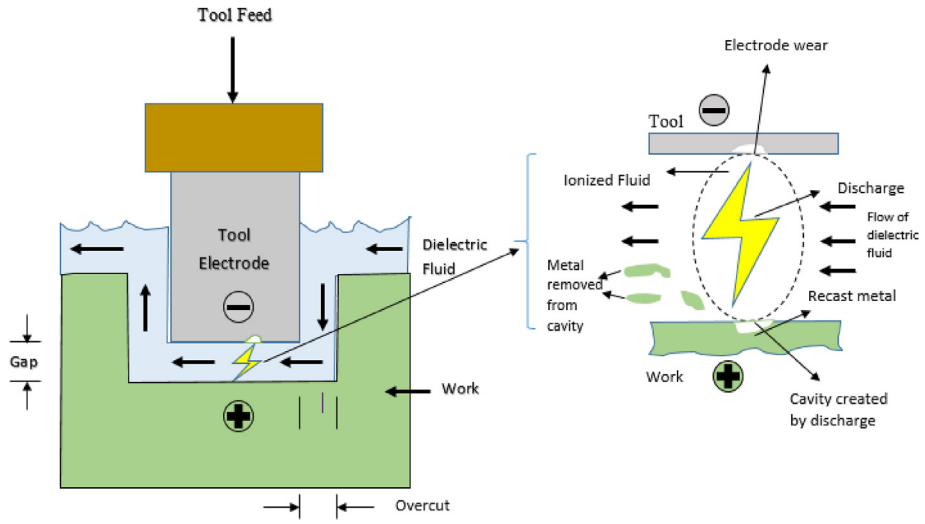


**Fig. 2.** Representation of tool-workpiece interface and machining zone in die-sinking EDM.

electrically conductive materials of any thermophysical, chemical, or mechanical properties. Material hardness has no effect on electric discharge machining; material toughness and hardness have no effect on power. Shape memory alloys come under the category of difficult-to-cut sophisticated materials, hence EDM is quite effective in machining them [23].

According to the reviewed literature, only few investigations on the machine learning based advanced optimization in EDM of shape memory alloy have been reported. The Cu-based SMA has been chosen as workpiece, as it has been very less explored and machined in the EDM process. Furthermore, the single and multi-objective machine learning based parametric optimization of response parameters such as TWR and DD has received little attention. According to the observations from the literature survey, a very few studies have attempted to choose TWR and DD as response parameters. TWR and DD have not been attempted to study while performing EDM operations on Cu-based SMA. So that's the reason behind the selection of DD and TWR as machining response parameters in this study. The simultaneous optimization of machining reactions will expand the process's applicability while addressing real-world industrial concerns.

Based on the above elaborations, it has been discovered that relatively few experimental research has been investigations on the machine learning based advanced optimization in EDM of shape memory alloy. Advanced machine learning based optimization approaches such as Genetic Algorithm and Teacher Learning Based Optimization have received less attention, therefore the required attempt is made to determine the influence of process parameters such as pulse on time, pulse off time, peak current, and gap voltage on tool wear rate and dimensional deviation and the simultaneous machine learning based optimization has also been attempted. In addition to this, the impact of machining inputs has also been investigated via the use of a variance test (ANOVA test).

## 2. Materials & methods

The Cu-based shape memory alloy was used as the work sample material for the Electric spark cut machining (ESCM) operations. Shape memory alloys are classified into three types: Based on the elements NiTi, Cu, and Fe. This examination focused on the existence of Cu content as a main component, although other elements such as Zn, Ni, Mn, Fe, and others were also included in the EDS analysis. To carry out the EDM operations, a Cu-based electrode was used as a tool. The workpiece is a disc with 110 × 20 mm. The diameter of the Cu electrode in EDM operations is 10 mm. Ton, Toff, Ip, and GV are the EDM process parameters used. TWR and DD are the response factors that are evaluated at various process parameter settings. Fig. 1 depicts the CNC EDM machine configuration used for the experimental work. It has many components such as a servo control mechanism, a tool post, a machining chamber with an air filter and a nozzle, an EDM regulating device, a visual monitoring screen, and a control unit.

Fig. 2 depicts an expanded view of the tool-workpiece interaction zone. The creation of spark has been depicted by its many features. The picture depicts tool feed movement, dielectric fluid, electrode wear, a cavity made in the workpiece, and metal removed from the cavity. Table 1 depicts the structure of Cu-based SMA.

Fig. 3 (a) shows the un-machined work sample's SEM micrograph and EDS analysis, whereas Fig. 3 (b) depicts the work sample disc of Cu-based SMA. Cu element has a higher percentage than the other major components. Table 2 summarizes the basic characteristics of Cu-based SMA.

Table 3 shows a variety of process parameters, together with their levels and measurements. Electric spark cut machining is a thermal technology that uses chosen pulsed releases that may be controlled temporally and spatially to treat electrically conductive materials independent of their thermo-physical, chemical, or mechanical properties [24]. In the 1940s, the EDM technique was found [25]. EDM is a cutting method that has been successfully used to cut difficult-to-cut materials [26]. The primary idea behind the EDM technique is to erode material off a workpiece using thermoelectric power and periodic electric discharges from an uncontacted electric electrode [27]. To immerse the tool and workpiece, a dielectric fluid is employed [28]. Conductive channels emerge as a result of the synthesis of electrons and positive ions during spark generation [29]. Ion collisions cause the formation of a high-temperature plasma channel [30]. Due to quick melting and evaporation, the workpiece is removed in the high temperature zone [31].

The main experiments were designed using the response surface methodology (RSM) [32]. RSM is a strategy for assessing relationships and performing optimization tests that focuses on the impact of

**Table 1**
Composition of Cu-based SMA.

| Element | Cu | Zn | Ni | Mn | Sn | Fe | Pb | P | Al |
|---|---|---|---|---|---|---|---|---|---|
| Composition(%) | 53.3 | 41.5 | 0.790 | 0.0480 | 0.338 | 0.233 | 3.56 | 0.0038 | <0.0020 |

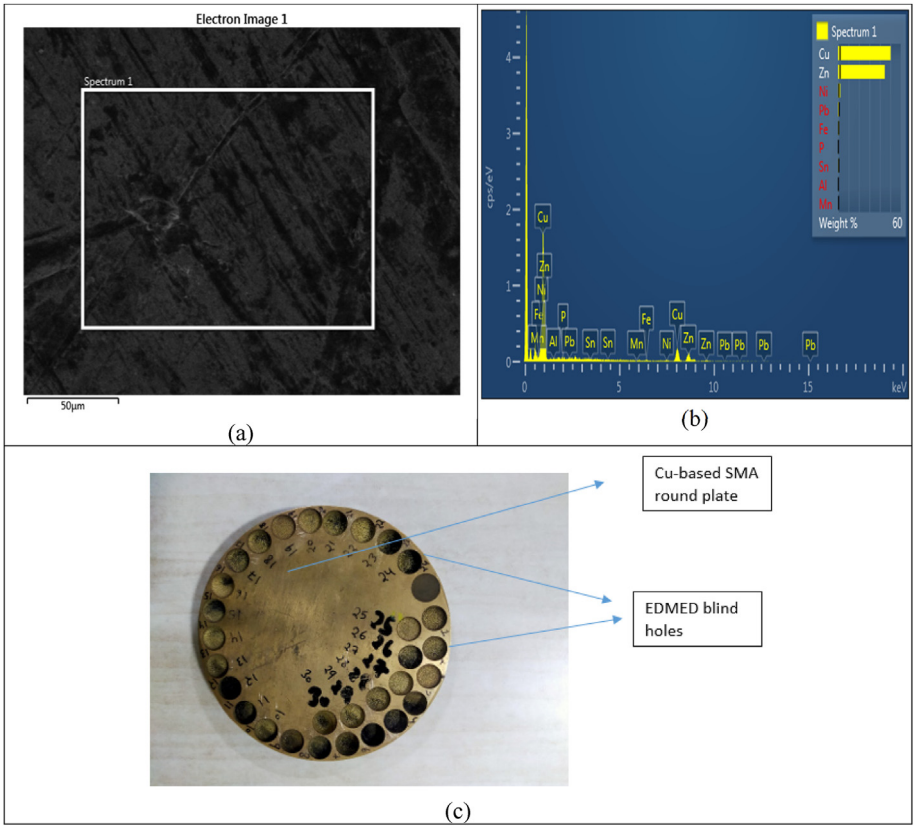


**Fig. 3.** (a) EDS analysis spectrum for Cu-based SMA (before machining) (b) EDMed Cu-based SMA work sample disc.

**Table 2**
Fundamental properties of Cu-based SMA.

| Terms | Units | Values |
|---|---|---|
| Martensite Young Modulus, $E_m$ | GPa | 16.5 |
| Austenite Young Modulus, $E_A$ | GPa | 40.2 |
| Ultimate elongation | % | 12.0 |
| Max (assumed) recoverable strain | % | 3.0 |
| Min necessary pre-load | Mpa | 155.6 |
| Martensite start temperature, $M_s$ | °C | 43.3 |
| Martensite finish temperature, $M_F$ | °C | 27.5 |
| Austenite start temperature, $M_s$ | °C | 47.3 |
| Austenite finish temperature, $M_F$ | °C | 58.9 |

numerous independent variables on a dependent variable or response [33]. Box and Wilson devised the concept in 1951 [34] while working on a chemical investigation. The RSM evaluates the relationship between controlled machining variables and response surfaces. This method is frequently used in agriculture, medicine, and industry, as well as in activities such as spinning, milling, cutting, riveting, press working, and extrusion. As shown by [35], the RSM strategy process is as follows:

1. Developing a series of research to analyse the response of interest in a reliable and acceptable way.
2. Creating a scientific model.
3. Determine the best experimental setup combination for obtaining the greatest or lowest response value.
4. The individual and cumulative impacts of process factors are shown in two- and three-dimensional graphs.

The response surface is the following when all the factors are deemed calculable:

$$z = \text{func}\ (g1, g2, g3, \ldots, gn) \tag{1}$$

where

z = yield response
$g_n$ = nth autonomous factor (Control factor)

The goal is to enhance z, the variable response. RSM involves fitting a mathematical model to the surface of a variable that is supposed to be dependent. In general, the following equations characterise RSM's second-order surface interactions.

$$z = \alpha_0 + \sum_{n=1}^{k} \alpha_n g_n + \sum_{n=1}^{k} \alpha_{nn} g_n^2 + \sum_{n<m} \alpha_{nm} g_n g_m + \omega \tag{2}$$

where

**Table 3**
Considered process parameters and their measures.

| Sr No. | Parameters | Symbol | Level 1 | Level 2 | Level 3 | Level 4 | Level 5 | Unit |
|---|---|---|---|---|---|---|---|---|
| 1 | Pulse on time | Ton | 35 | 90 | 145 | 200 | 255 | µs |
| 2 | Pulse off time | Toff | 15 | 60 | 105 | 150 | 195 | µs |
| 3 | Peak current | Ip | 10 | 20 | 30 | 40 | 50 | Amp |
| 4 | Gap voltage | GV | 15 | 30 | 45 | 60 | 75 | Volt |

**Table 4**
Control log for main experimentation.

| Std | Run | Pulse on time (μs) | Pulse off time (μs) | Peak current (A) | Gap voltage (V) | TWR (g/min) | DD (mm) |
|---|---|---|---|---|---|---|---|
| 16 | 1 | 200 | 150 | 40 | 60 | 0.7158 | 0.05 |
| 25 | 2 | 145 | 105 | 30 | 45 | 0.5193 | 0.06 |
| 7 | 3 | 90 | 150 | 40 | 30 | 0.3685 | 0.09 |
| 19 | 4 | 145 | 15 | 30 | 45 | 0.6143 | 0.092 |
| 4 | 5 | 200 | 150 | 20 | 30 | 0.6525 | 0.04 |
| 21 | 6 | 145 | 105 | 10 | 45 | 0.3823 | 0.09 |
| 14 | 7 | 200 | 60 | 40 | 60 | 0.8209 | 0.12 |
| 3 | 8 | 90 | 150 | 20 | 30 | 0.1868 | 0.06 |
| 22 | 9 | 145 | 105 | 50 | 45 | 0.6753 | 0.16 |
| 29 | 10 | 145 | 105 | 30 | 45 | 0.5165 | 0.04 |
| 12 | 11 | 200 | 150 | 20 | 60 | 0.6178 | 0.04 |
| 2 | 12 | 200 | 60 | 20 | 30 | 0.7603 | 0.11 |
| 28 | 13 | 145 | 105 | 30 | 45 | 0.5181 | 0.05 |
| 27 | 14 | 145 | 105 | 30 | 45 | 0.5159 | 0.047 |
| 1 | 15 | 90 | 60 | 20 | 30 | 0.2693 | 0.03 |
| 13 | 16 | 90 | 60 | 40 | 60 | 0.4157 | 0.05 |
| 24 | 17 | 145 | 105 | 30 | 75 | 0.4704 | 0.02 |
| 26 | 18 | 145 | 105 | 30 | 45 | 0.5176 | 0.06 |
| 15 | 19 | 90 | 150 | 40 | 60 | 0.3247 | 0.04 |
| 20 | 20 | 145 | 195 | 30 | 45 | 0.4209 | 0.03 |
| 18 | 21 | 255 | 105 | 30 | 45 | 0.9526 | 0.08 |
| 8 | 22 | 200 | 150 | 40 | 30 | 0.7529 | 0.09 |
| 6 | 23 | 200 | 60 | 40 | 30 | 0.8493 | 0.18 |
| 10 | 24 | 200 | 60 | 20 | 60 | 0.7170 | 0.13 |
| 17 | 25 | 35 | 105 | 30 | 45 | 0.0820 | 0.02 |
| 9 | 26 | 90 | 60 | 20 | 60 | 0.2327 | 0.042 |
| 11 | 27 | 90 | 150 | 20 | 60 | 0.1388 | 0.04 |
| 23 | 28 | 145 | 105 | 30 | 15 | 0.5626 | 0.1 |
| 30 | 29 | 145 | 105 | 30 | 45 | 0.5128 | 0.04 |
| 5 | 30 | 90 | 60 | 40 | 30 | 0.4648 | 0.11 |

**Table 5**
ANOVA for tool wear rate (TWR).

| Source | Sum of Squares | DF | Mean Square | F Value | Prob > F |
|---|---|---|---|---|---|
| Model | 1.336861 | 8 | 0.167108 | 14076.51 | <0.0001[a] |
| A | 1.138233 | 1 | 1.138233 | 95880.41 | <0.0001[a] |
| B | 0.055968 | 1 | 0.055968 | 4714.49 | <0.0001[a] |
| C | 0.12374 | 1 | 0.12374 | 10423.37 | <0.0001[a] |
| D | 0.010641 | 1 | 0.010641 | 896.3666 | <0.0001[a] |
| C2 | 0.000219 | 1 | 0.000219 | 18.4084 | 0.0003[a] |
| AB | 0.000125 | 1 | 0.000125 | 10.55904 | 0.0038[a] |
| AC | 0.007864 | 1 | 0.007864 | 662.4377 | <0.0001[a] |
| Residual | 7.17E-05 | 1 | 7.17E-05 | | |
| Lack of Fit | 0.000249 | 21 | 1.19E-05 | 2.73856 | 0.1351[b] |
| Pure Error | 0.000224 | 16 | 1.4E-05 | | |
| Cor Total | 2.55E-05 | 5 | | | |
| **Std. Dev.** | 0.003445 | | | **R-Squared** | 0.999814 |
| **Mean** | 0.518322 | | | **Adj R-Squared** | 0.999743 |
| **C.V.** | 0.664739 | | | **Pred R-Squared** | 0.999523 |
| **PRESS** | 0.000637 | | | **Adeq Precision** | 461.5924 |

A-Pulse on Time; B-Pulse off Time; C-Peak Current; D-Gap Voltage.
[a] Significant.
[b] Not-Significant.

$z$ = yield response
$g_n$ = nth controller factor
$\alpha$ = coefficient of regression
$\omega$ = arbitrary error

The experiments were evaluated using the RSM technique, which is the Central Composite Design, in order to build an experimental design that produced great findings (CCD). Table 4 shows the major experimentation's Design of Experiment.

**Table 6**
ANOVA table for dimensional deviation.

| Source | Sum of Squares | DF | Mean Square | F Value | Prob > F |
|---|---|---|---|---|---|
| A | 0.046134 | 7 | 0.006591 | 58.9675 | <0.0001[a] |
| B | 0.00728 | 1 | 0.00728 | 65.13734 | <0.0001[a] |
| C | 0.008288 | 1 | 0.008288 | 74.15615 | <0.0001[a] |
| D | 0.005954 | 1 | 0.005954 | 53.26734 | <0.0001[a] |
| $C^2$ | 0.00534 | 1 | 0.00534 | 47.77971 | <0.0001[a] |
| AB | 0.009872 | 1 | 0.009872 | 88.32354 | <0.0001[a] |
| CD | 0.00632 | 1 | 0.00632 | 56.54874 | <0.0001[a] |
| A | 0.00308 | 1 | 0.00308 | 27.55971 | <0.0001[a] |
| B | 0.002459 | 22 | 0.000112 | 58.9675 | <0.0001[a] |
| Residual | 0.002051 | 17 | 0.000121 | | |
| Lack of Fit | 0.000408 | 5 | 8.15E-05 | 1.48 | 0.3522[b] |
| Pure Error | 0.048593 | 29 | 0.006591 | | |
| Cor Total | 0.046134 | 7 | | | |
| **Std. Dev.** | 0.010572 | | | **R-Squared** | 0.949399 |
| **Mean** | 0.070367 | | | **Adj R-Squared** | 0.933298 |
| **C.V.** | 15.02411 | | | **Pred R-Squared** | 0.904076 |
| **PRESS** | 0.004661 | | | **Adeq Precision** | 28.5927 |

A-Pulse on Time; B-Pulse off Time; C-Peak Current; D-Gap Voltage.
[a] Significant.
[b] Not-Significant.

## 3. Results and discussions

The output response factors are TWR and DD. The ANOVA findings for the output responses are shown in Tables 5 and 6. According to the testing findings, the F-values for the TWR and DD models are 14076.51 and 58.97, respectively, showing that the model is extremely significant. Calculating the Model F value yields this very significant result, which is extremely unlikely to occur due to noise.

Variables with probability larger than F values less than 0.05 are more likely to be significant. The presence of factors with values larger than 0.1000 is not statistically significant. The lack-of-fit tests compare the residual error to the pure error from replicated design points. A lack-of-fit error significantly larger than the pure error indicates that something remains in the residuals that can be removed by a more appropriate model. If it has been seen that the significant lack-of-fit (Prob > F value 0.10 or smaller) then don't use the model as a predictor of the response [36]. The F-values of 2.74 and 1.48 for the TWR and DD, respectively, are lower than the pure error, indicating that the lack of fit (LOF) is not statistically significant. Due to random fluctuations, an F-value of LOF of this magnitude has a 13.51% chance of happening in the case of TWR and a 35.22% chance of occurring in the event of DD. The lack of a poor fit indicates that the model is excellent.

### 3.1. Regression equation for TWR and DD

$$\textbf{TWR} = -0.24861 + 0.00517211 * \text{Ton} - 0.000909140 * \text{Toff} + 0.011372 * \text{Ip} - 0.00177584 * \text{GV} + 0.0000275461 * \text{Ip}^2 - 0.00000113092 * \text{Ton} * \text{Toff} - 0.0000403089 * \text{Ton} * \text{Ip} + 0.00000256594 * \text{Ton} * \text{GV} \quad \ldots(3)$$

$$\textbf{Dimensional deviation (DD)} = -0.030011 + 0.00115985 * \text{Ton} + 0.000751431 * \text{Toff} - 0.00537083 * \text{Ip} + 0.00178056 * \text{GV} + 0.000185139 * \text{Ip}^2 - 0.00000803030 * \text{Ton} * \text{Toff} - 0.0000925000 * \text{Ip} * \text{GV} \quad (4)$$

Fig. 4 shows predicted v/s. TWR (g/min) actual plot (b) Dimensional Deviation (mm). All of the data lie along a straight line, indicating that the model is acceptable. Fig. 5 displays a 2D representation of the influence of several process parameters on the TWR and DD, such as pulse on time (Ton), pulse off time (Toff), peak current (Ip), and gap voltage (GV). As the pulse rate rises, so does the TWR. Because there is less time lag between the pulses, more sparks appear as the pulse frequency rises.

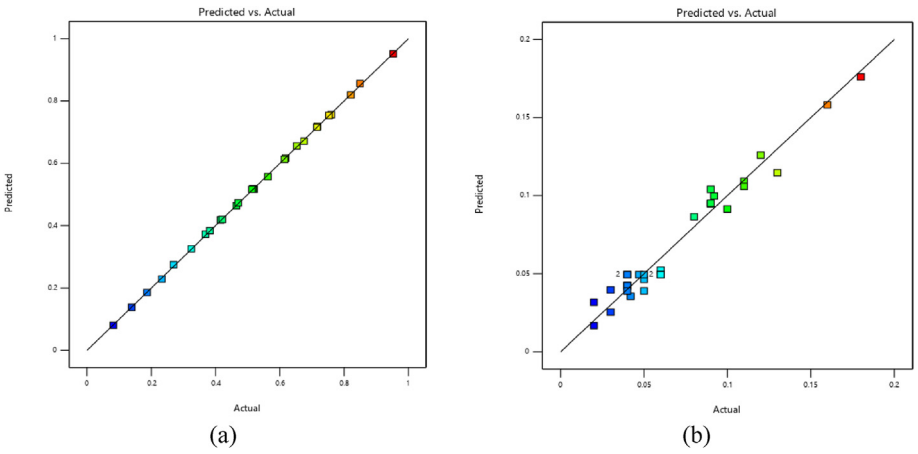


**Fig. 4.** Predicted v/s Actual plot for (a) TWR (g/min) (b) Dimensional Deviation (mm).

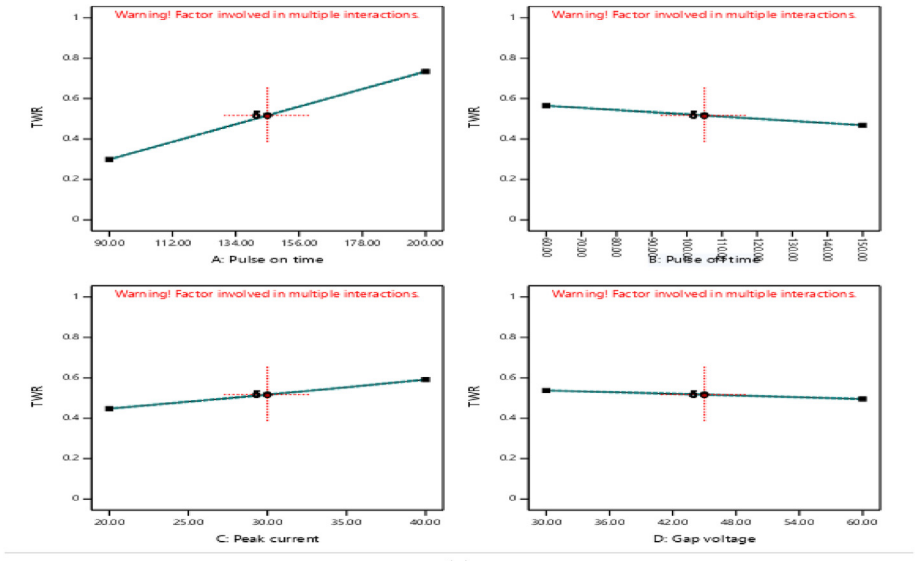


**Fig. 5.** Single factor effects of considered EDM inputs on (a) TWR (g/min) (b) Dimensional Deviation (mm).

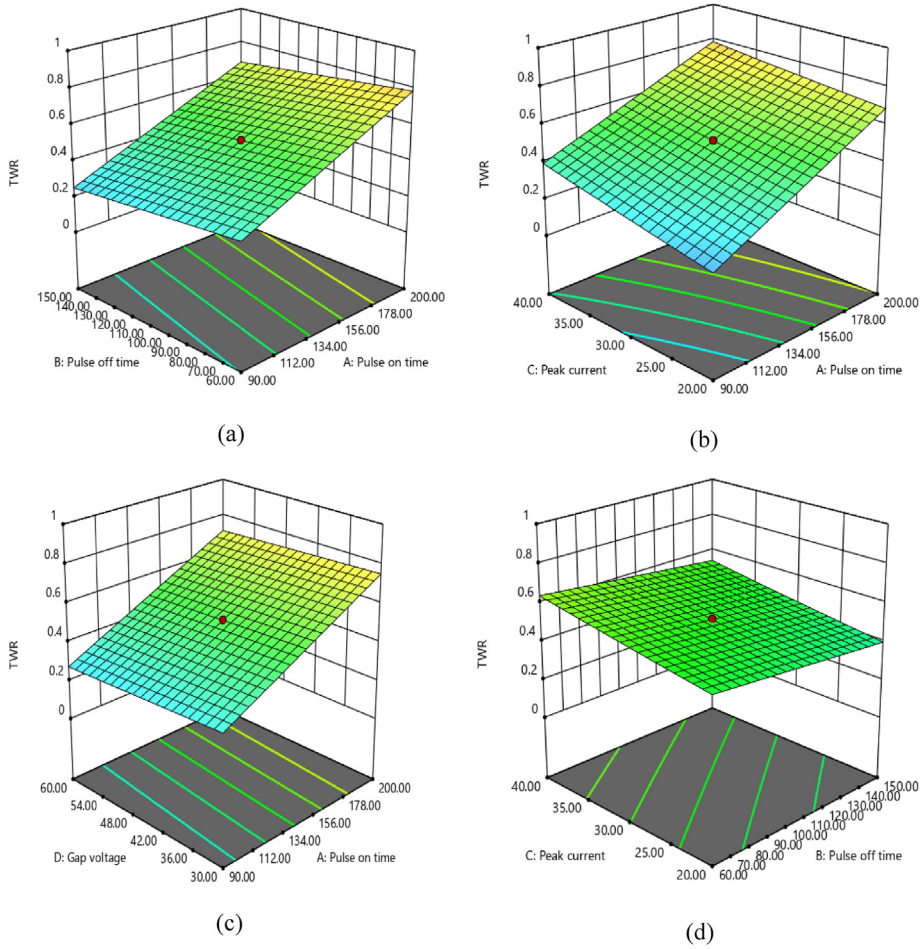


**Fig. 6.** 3D interactive effects of studied EDM inputs on TWR (g/min) (a) TWR vs Ton and Toff (b) TWR vs Ip and Ton (c) TWR vs GV and Ton (d)TWR vs Ip and Toff.

The tool-to-work contact gets heated as a result of the huge spark creation. Because of the high temperature, the tool's surface melts and evaporates more rapidly. When the tool surface melts and evaporates more, TWR rises. As the pulse off time grows, TWR falls [37]. As the pulse off time increases, so does the length between pulses, which minimizes spark creation since there is less time between them. The lower the temperature at the created machining contact, the fewer sparks produced. The substance on the work surface does not melt or evaporate as much because to the low temperature. The quantity of material removed from the work surface causes TWR to drop in direct proportion [38]. The TWR rises as peak current increases. When the maximum current increases, more current flows through, resulting in high temperatures. As a result of the higher TWR produced by the high temperature formation. TWR drops as the gap voltage rises. As the gap voltage increases, so does the discharge waiting time, which lowers spark creation and, as a consequence, temperature accumulation. As a result of the lower temperature formation, TWR is lowered. An increase in the pulse on time causes the value of dimensional deviation to rise. More sparks develop when the time gap between pulse occurrences decreases. Increasing the spark production causes the temperature to rise, removing more material [39]. As a consequence of the significant material removal, the required sample has more dimensional variance. The increase in pulse off time is responsible for the decrease in dimensional deviation [40]. Because there is greater time passed between pulses as the pulse off time grows, there is less time to form sparks. The lower the temperature at the tool-work contact, the fewer sparks produced. Less material is eliminated due to the low temperature [41]. The lower quantity of material eliminated results in less dimensional variation. As peak current increases, so does dimensional deviation [42]. As the peak current rises, so does the current. More heat is created as the current rises. The melting and evaporation processes remove more material as the temperature rises. As the quantity of material removed increases, the dimensions of the samples deform [43]. The dimensional divergence worsens as the peak current increases [44]. An increase in gap voltage causes the decrease in dimensional deviation. Increased gap voltage leads in a longer discharge waiting time, which results in less spark creation and, thus, less temperature formation. Lower temperatures result in less dimensional fluctuation [45].

Fig. 6 depicts 3D graphs that highlight the link between process parameters and the response parameter (i.e. TWR). TWR decreases as the pulse off time increases. TWR climbs when Pulse rises in real time. The TWR increases in response to an increase in the Peak current. As the pulse off time grows, TWR falls. As the Gap voltage increases, the TWR lowers [46]. The increase in TWR value is the result of an increase in Pulse over time [47]. The TWR value drops as the gap voltage rises. The TWR's value grows in tandem with the increase in peak current value.

Fig. 7 depicts the effect of process parameter combinations on dimensional deviation. Dimensional deviation is decreased by increasing the pulse off time. As the pulse rate increases with time, so does the dimension deviation. The rise in pulse on time is exactly proportional to the increase in dimensional deviation [48]. As peak current increases, so does dimensional deviation. When the pulse on time grows, so does the dimensional divergence. As the gap voltage increases, the value of dimensional deviation falls [49]. The dimensional deviation increases as the maximum current increases. Increases in pulse off time result in a reduction in dimensional deviation value.

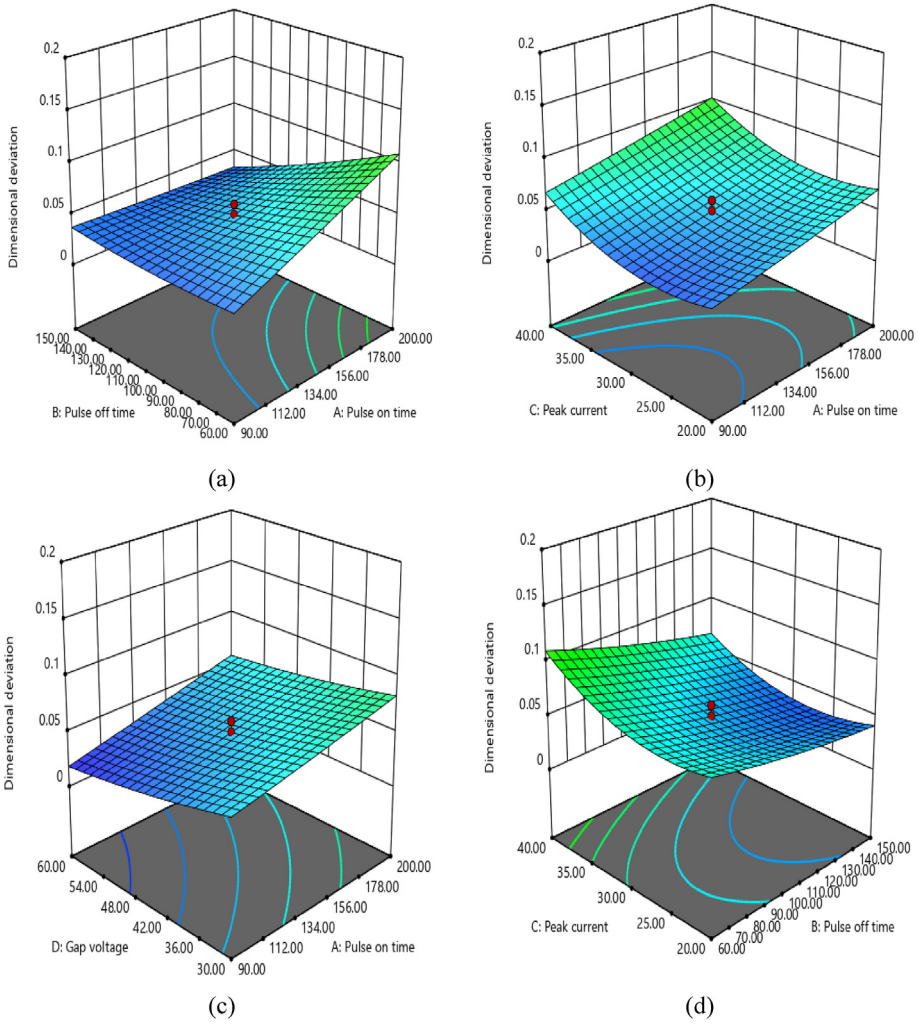


**Fig. 7.** 3D interactive effects of studied EDM inputs on DD(mm) (a) DD vs Toff and Ton (b) DD vs Ip and Ton (c) DD vs GV and Ton (d) DD vs Ip and Toff.

**Table 7**
Single response optimization (for TWR and DD) using Desirability, GA, and TLBO methods.

| S. No. | Optimization | Response(s) | Optimized conditions | | | | Predicted values | Confirmatory results | Best experimental results |
|---|---|---|---|---|---|---|---|---|---|
| | | | Pulse on time (μm) | Pulse off time (μm) | Peak current (A) | Gap voltage (V) | | | |
| 1. | Desirability Approach | TWR (g/min) | **90.00** | **150.00** | **20.07** | **60.00** | 0.13912 | 0.14254 | 0.13889 |
| | | Dimensional Deviation (μm) | **198.28** | **149.81** | **28.88** | **59.91** | 0.0199343 | 0.02012 | 0.02 |
| 2. | Genetic Algorithm | TWR (g/min) | **35.00** | **195.00** | **10.00** | **72.34** | 0.0000 | 0.2845 | 0.13889 |
| | | Dimensional Deviation (μm) | **255.00** | **195.00** | **33.24** | **75.00** | 0.0000 | 0.062 | 0.02 |
| 3. | TLBO | TWR (g/min) | **35.00** | **195.00** | **10.00** | **75.00** | 0.0000 | 530.523 | 0.13889 |
| | | Dimensional Deviation (μm) | **35.00** | **15.00** | **33.26** | **75.00** | 0.0000 | 0.0623 | 0.02 |

## 4. Machine learning (ML) based parametric optimization for single and multiple responses (both TWR and DD)

### 4.1. Single response optimization

The response parameters explored in this study, TWR and DD, in the EDM approach, are extremely disputed in nature. At various parametric combinations, it is impossible to achieve both a low TWR and a low dimensional deviation. For industrial applications, it is critical to provide machining outcomes capable of achieving many objectives at the same time. The desirability method, Genetic algorithm, and TLBO were utilised for single response optimization to get optimal outcomes, as reflected in Table 7.

### 4.2. Using desirability approach

The desirability approach is a common way for assigning a "score" to a collection of replies and selecting factor settings that maximize that score. The desirability approach normalises a response estimate by transforming it into a scale-free value called desirability [50]. By maximising, reducing, or obtaining the desired value of a response, optimization objectives may be utilised to raise, decrease, or accomplish it [51].

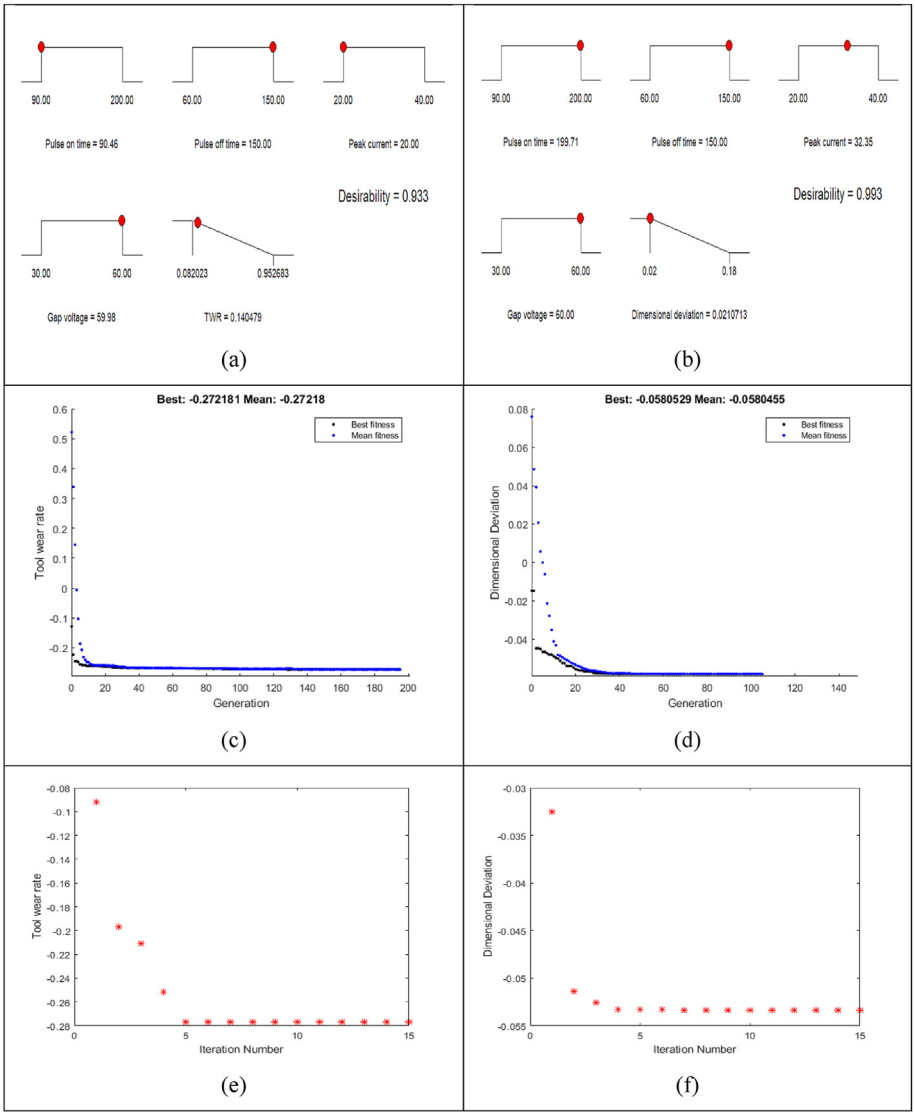


**Fig. 8.** Single Measure Optimization of TWR (g/min), and DD (mm); (a & b) using Desirability Approach; (c & d) using Genetic algorithm, and (e & f) using TLBO, respectively.

Depending on the aims, many functions may be used [52]. Fig. 8 depicts the Single Measure Optimization of TWR (g/min) and DD (mm) using the Desirability Approach (a & b), the Genetic Algorithm (c & d), and the TLBO (e & f), respectively. The optimum TWR value is 0.13912 g/min, while the optimized DD value is 0.0199343 mm.

### 4.3. Using genetic algorithm (GA)

Genetic Algorithms (GAs) are adaptive heuristic search algorithms that are a subset of evolutionary algorithms. Natural selection and genetics are the foundations of genetic algorithms. These are intelligent uses of random search supplied with historical data to lead the search towards the area of greater performance in the solution space. They are often utilised to provide high-quality solutions to optimization and search challenges. For single goal optimization, a genetic algorithm is used in this section [53]. The optimization tool in MATLAB v14 is used for GA implementation [54]. The parameters of GA have been kept at their default values [55]. The optimal TWR value in the case of TWR is −0.2722; obtained at Ton (35), pulse-Toff time (195), Ip (10) and GV (72.34). In the case of DD, the best value obtained after GA is a -ve numerical value (i.e., −0.058) at Ton (255), Toff (195), Ip (33.24), and GV (75). The experiment indicates that the negative value of DD at the optimum process variable setting means that DD will be either zero or minimum at this configuration.

### 4.4. Using TLBO

The Teaching–Learning–Based Optimization (TLBO) method is suggested for obtaining global solutions for continuous nonlinear functions with little computing effort and great consistency. The TLBO approach is based on the impact of a teacher's influence on the production of students in a class. Another modern optimization approach (TLBO) is used for single objective optimization in this section [56]. There are several different forms of TLBO that may be used for optimization [57]. TLBO is used in this study because of its accuracy and convenience of usage [58]. The technique is written in MATLAB v14 and is used to implement the s-TLBO on both responses. The optimal value in the context of TWR is 0.03295, which was obtained at Ton (35), Toff (195), Ip (10) and GV (33.3). In the case of DD, the best value obtained by using this approach is a -ve numeric value (i.e., −0.0403) at Ton (35), Toff (195), Ip (10), and GV (46.8). The experiment indicates that the negative value of DD at the optimum process variable setting means that DD will be either zero or minimum at this configuration. Fig. 9 depicts the TLBO Technique's procedural flowchart.

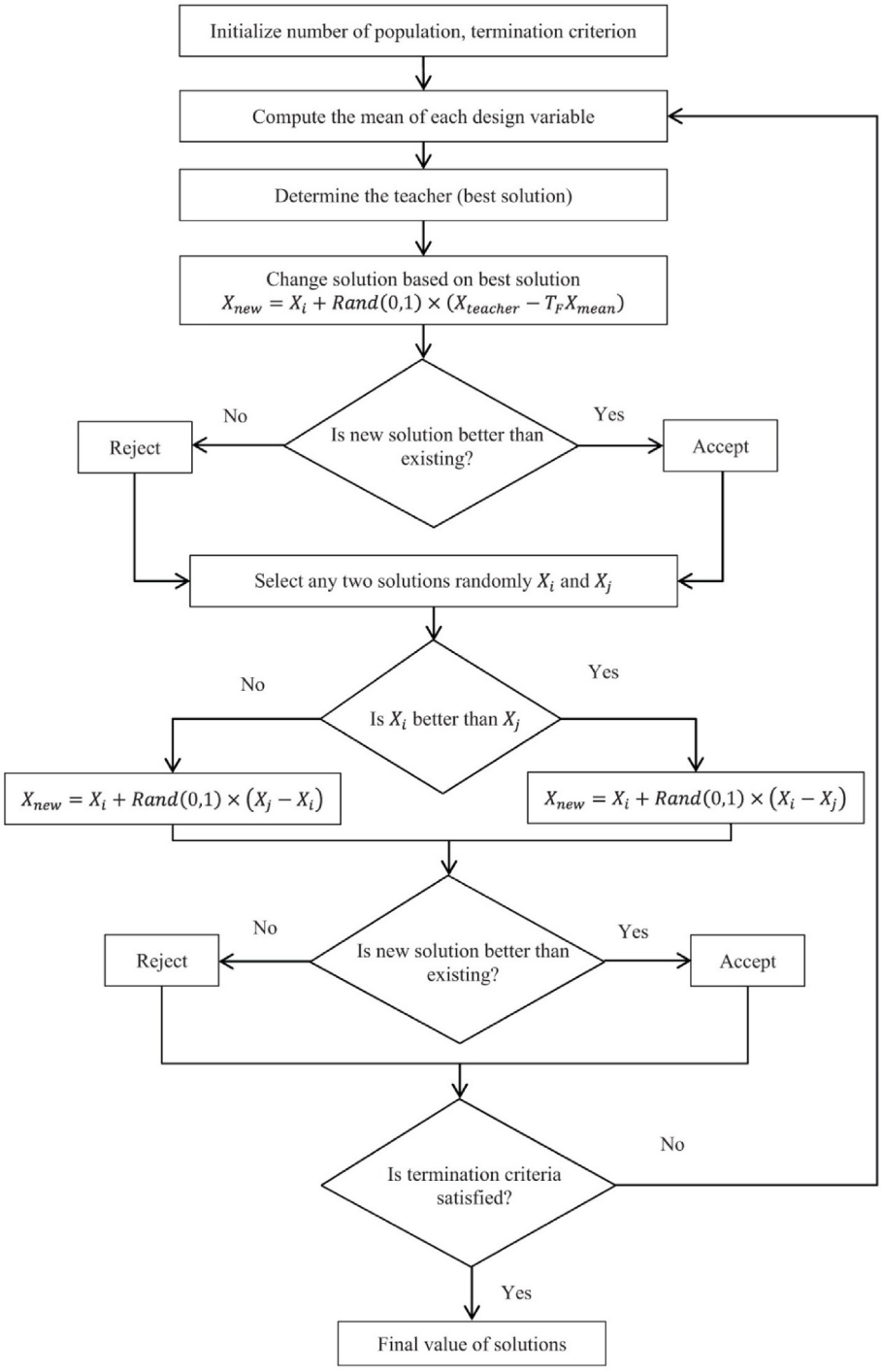


**Fig. 9.** Procedural flowchart for TLBO.

## 5. Multi-response optimization

### 5.1. Using desirability approach

Fig. 10 shows the Multi-Objective Optimization of TWR (g/min) and DD (mm); (a & b) using Desirability Approach; (c & d) using Genetic Algorithm; and (e & f) using TLBO, respectively. The optimum TWR value is 0.076 g/min, while the optimized DD value is 0.0479 mm. Desirability has an overall rating of 0.865.

### 5.2. Multi-objective optimization (MOOPs)

As a result of the one response, the other response is affected as well. As a result, it is essential to optimise replies simultaneously [59]. Priory method is used to create a single objective function to maximize the different answers concurrently [60]. The MOOPs is determined by the TWR and DD (Eq. (5)). Eq (6) shows the objective function for the MOOPs, which assigns a weight of 0.5 to both replies. Using GA and TLBO, the minimum values of both the responses (i.e., TWR and DD) are

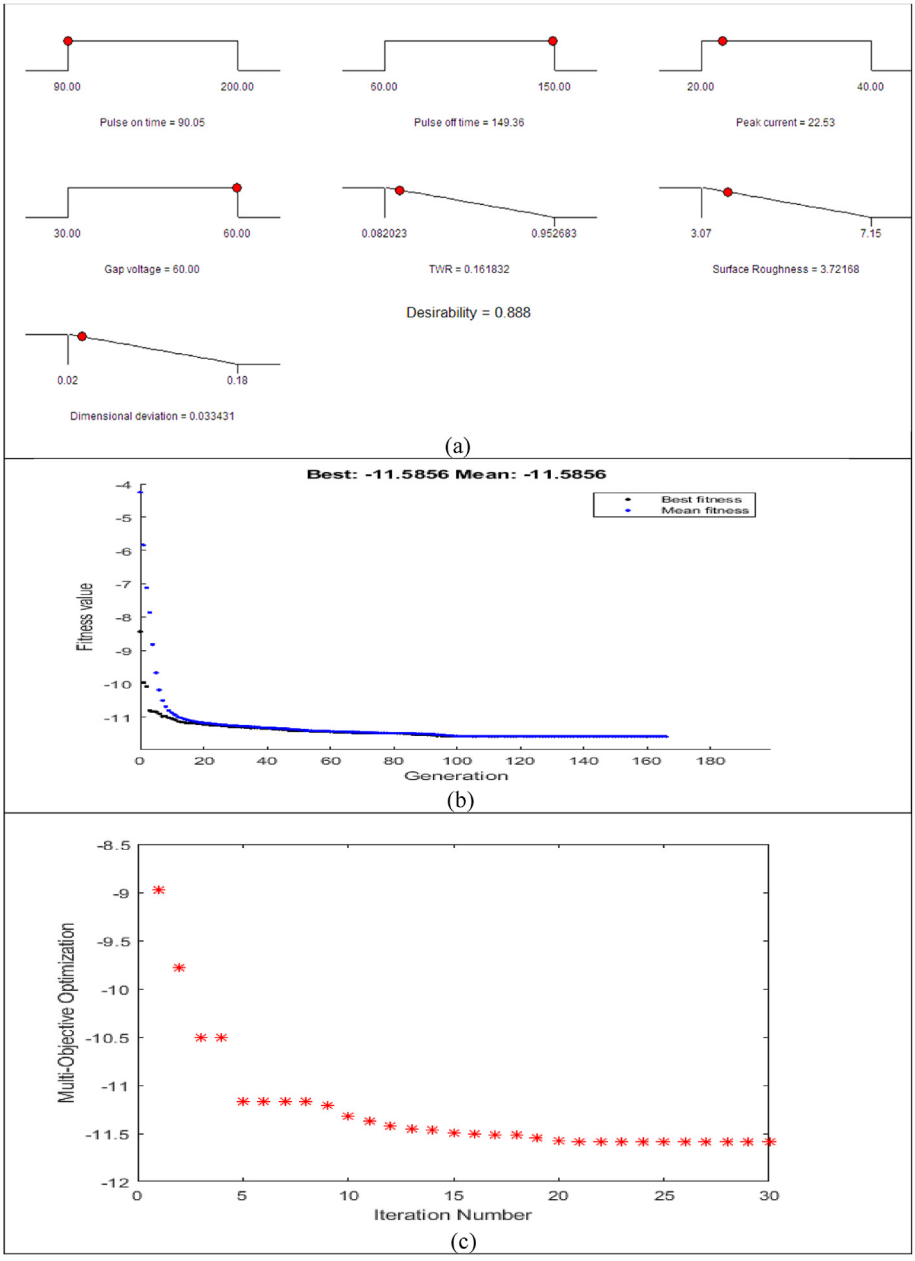


**Fig. 10.** Multi-Objective Optimization of TWR (g/min), and DD (mm); (a & b) using Desirability Approach; (c & d) using Genetic algorithm, and (e & f) using TLBO, respectively.

**Table 8**
Multi-response optimization of machining responses i.e., TWR and DD using desirability, Genetic Algorithm and TLBO methods.

| S. No. | Optimization | Response(s) | Optimized conditions | | | | Predicted values | Confirmatory results | Best experimental results |
|---|---|---|---|---|---|---|---|---|---|
| | | | Pulse on time (μm) | Pulse off time (μm) | Peak current (A) | Gap voltage (V) | | | |
| 1. | Desirability Approach | TWR (g/min)<br>Dimensional Deviation (μm) | **90.10** | **149.69** | **24.59** | **60.00** | 0.180361<br>0.0289 | 0.1982<br>4.80 | 0.13889<br>0.02 |
| 2. | Genetic Algorithm | TWR (g/min)<br>Dimensional Deviation (μm) | **255.00** | **15.00** | **50.00** | **15.00** | 0.410<br>0.0541 | 0.452<br>0.0565 | 0.13889<br>0.02 |
| 3. | TLBO | TWR (g/min)<br>Dimensional Deviation (μm) | **255.00** | **15.00** | **50.00** | **15.00** | 0.4103<br>0.054 | 0.422<br>0.0565 | 0.13889<br>0.02 |

used as achieved in the single optimization step. Table 8 contains the optimal settings and optimized values after employing GA and TLBO. The tests conducted under these conditions.

$$MOOPs = f(TWR, DD \tag{5}$$

$$MOOPs = w(\frac{TWR}{TWR_{min}}) + w(\frac{DD}{DD_{min}}) \tag{6}$$

## 6. Conclusions

The attempt has been made to experimentally investigate the impact of the selected EDM process inputs and to optimize the considered responses by using the machine learning based algorithms such as; genetic algorithm (GA), and TLBO technique. The major findings are as follows:

1. The pulse off time, pulse on time, and peak current have been shown to be the most important factors for the investigated response parameters, TWR and DD, in Cu-based SMA EDM. TWR is highest in different operations when long pulse on times and large peak currents are employed. As the pulse off time grows, the TWR value decreases, and vice versa for decreasing pulse off time values. Lowering the DD was accomplished by lowering the peak current and pulse on time values.
2. In terms of TWR, the bigger the pulse off time and the lower the pulse on time and peak current, the better the solution. It has been discovered that as the pulse off time grows, so does the time lag between pulse occurrences. High temperatures cause the tool electrode to melt and evaporate more quickly, resulting in a high TWR. Because of the strong current, high temperatures occur, causing additional erosion of the tool surface. The tool's substantial deterioration results in a considerable TWR.
3. In terms of dimensional deviation, a lower Ton and Ip with a higher Toff is the best answer. The longer the time lag between pulse occurrences, the bigger the time lag between pulse occurrences, resulting in less spark creation. The less material removed, the finer the machining, the less departure from the product's true shape, and, ultimately, the smaller the DD.
4. The optimum combination of parameters for the TWR was developed as; Ton = 90.00 μs, Toff = 150 μs, Ip = 20.07 A, GV = 60.00 V; Ton = 35 μs, Toff = 195 μs, Ip = 10 A, GV = 72.34 V; Ton = 35 μs, Toff = 195 μs, Ip = 10 A, GV = 75 V in case of desirabity approach, Genetic Algorithm (GA), and TLBO, respectively. The best parametric combination for the DD was devised as; Ton = 198.28 μs, Toff = 149.81 μs, Ip = 28.88 A, GV = 59.91; Ton = 255 μs, Toff = 195 μs, Ip = 33.24 A, GV = 75 V; Ton = 35 μs, Toff = 15 μs, Ip = 33.26 A, GV = 75.00 V in case of desirabity approach, Genetic Algorithm (GA), and TLBO, respectively.
5. The parametric combination attained for optimization of multiple responses (TWR and DD) is: Ton = 90.10 μs, Toff = 149.69 μs, Ip = 24.59 A & GV = 60 V; Ton = 255 μs, Toff = 15 μs, Ip = 50 A & GV = 15 V; Ton = 255 μs, Toff = 15 μs, Ip = 50 A & GV = 15 V using desirability approach, GA method and TLBO method, respectively. The value of confirmatory experiments for the TWR and dimensional deviation is 0.180361 g/min and 0.0289 mm; 0.410 g/min and 0.0541 mm; 0.4103 g/min and 0.054 mm using desirability approach, GA method and TLBO method.
6. The present investigation has been attempted by considering the four available EDM input factors. However, more number of process inputs can be included in the future research studies based on the availability and functionality of the EDM set-up. The present work was limited to the Electrical Discharge Machining of Cu-based shape memory alloy, some more advanced materials based on the available literature can be machined to explore the capability of the EDM process. In addition to this, the surface morphology and topography based issues will be of paramount importance for future research investigations.

## Declaration of competing interest

The authors declare that they have no known competing financial interests or personal relationships that could have appeared to influence the work reported in this paper.

## References


[1] J.M. Jani, M. Leary, A. Subic, et al., A review of shape memory alloy research, applications and opportunities, Mater. Des. 56 (1980–2015) (2014) 1078–1113.
[2] L. Sun, W.M. Huang, Z. Ding, et al., Stimulus-responsive shape memory materials: a review, Mater. Des. 33 (2012) 577–640.
[3] R. Singh, R.P. Singh, R. Trehan, State of the art in processing of shape memory alloys with electrical discharge machining: a review, Proc. IME B: J. Eng. Manufact. 235 (3) (2021) 333–366.
[4] R.P. Singh, S. Singhal, Investigation of machining characteristics in rotary ultrasonic machining of alumina ceramic, Mater. Manuf. Process. 32 (3) (2017) 309–326.
[5] R. Chaudhari, J.J. Vora, V. Patel, L.N. Lacalle, D.M. Parikh, Effect of WEDM process parameters on surface morphology of nitinol shape memory alloy, Materials 13 (21) (2020) 4943. Jan.
[6] R. Chaudhari, P. Prajapati, S. Khanna, J. Vora, V.K. Patel, D.Y. Pimenov, K. Giasin, Multi-response optimization of Al2O3 nanopowder-mixed wire electrical discharge machining process parameters of nitinol shape memory alloy, Materials 15 (6) (2022), 2018.
[7] R. Chaudhari, J.J. Vora, S.S. Mani Prabu, I.A. Palani, V.K. Patel, D.M. Parikh, L.N. de Lacalle, Multi-response optimization of WEDM process parameters for machining of superelastic nitinol shape-memory alloy using a heat-transfer search algorithm, Materials 12 (8) (2019) 1277. Jan.
[8] N. Tosun, C. Cogun, Analysis of wire erosion and workpiece surface roughness in wire electrical discharge machining, Proc. IME B: J. Eng. Manufact. 217 (5) (2003) 633–642.
[9] S. Jain, V. Parashar, Critical review on the impact of EDM process on biomedical materials, Mater. Manuf. Process. (2021) 1–24, https://doi.org/10.1080/10426914.2021.1942907.
[10] Q. Kong, G. Liu, X. Fan, et al., A nested circle-fitting method for micro-hole centering and its application in electrochemical deburring, Proc. IME B: J. Eng. Manufact. 233 (12) (2019) 2292–2305.
[11] R. Singh, R.P. Singh, R. Trehan, Parametric investigation of tool wear rate in EDM of Fe-based shape memory alloy: microstructural analysis and optimization using genetic algorithm, World J. Eng. (2021), https://doi.org/10.1108/WJE-04-2021-0203.
[12] R. Singh, A. Dvivedi, P. Kumar, EDM of high aspect ratio micro-holes on Ti-6Al-4V alloy by synchronizing energy interactions, Mater. Manuf. Process. 35 (11) (2020) 1188–1203.
[13] J.E. Abu Qudeiri, A.H.I. Mourad, A. Ziout, et al., Electric discharge machining of titanium and its alloys: review, Int. J. Adv. Manuf. Technol. 96 (1–4) (2018) 1319–1339.
[14] N. Sharma, T. Raj, K.K. Jangra, Parameter optimization and experimental study on wire electrical discharge machining of porous Ni40Ti60 alloy, Proc. IME B: Eng. Manuf. 231 (6) (2017) 956–970.
[15] P. Mandal, S.C. Mondal, Surface characteristics of mild steel using EDM with Cu-MWCNT composite electrode, Mater. Manuf. Process. 34 (12) (2019) 1326–1332.
[16] A. Alidoosti, A. Ghafari-Nazari, F. Moztarzadeh, et al., Electrical discharge machining characteristics of nickel titanium shape memory alloy based on full factorial design, J. Intell. Mater. Syst. Struct. 24 (13) (2013) 1546–1556.
[17] M.H. Abidi, A.M. Al-Ahmari, U. Umer, et al., Multi-objective optimization of micro-electrical discharge machining of nickel-titanium-based shape memory alloy using MOGA-II, Meas. 125 (2018) 336–349.
[18] M.U. Gaikwad, A. Krishnamoorthy, V.S. Jatti, Investigation and optimization of process parameters in electrical discharge machining (EDM) process for NiTi 60, Mater. Res. Express 6 (6) (2019), 065707.
[19] S. Daneshmand, E.F. Kahrizi, E. Abedi, et al., Influence of machining parameters on electro discharge machining of NiTi shape memory alloys, Int. J. Electrochem. Sci. 8 (3) (2013) 3095–3104.
[20] V. Gaikwad, V.K.S. Jatti, Optimization of material removal rate during electrical discharge machining of cryo-treated NiTi alloys using Taguchi's method, J. Eng. Sci. King Saud Univ. 30 (3) (2018) 266–272.
[21] A.P. Dwivedi, S.K. Choudhury, Effect of tool rotation on MRR, TWR, and surface integrity of AISI-D3 steel using the rotary EDM process, Mater. Manuf. Process. 31 (14) (2016) 1844–1852.
[22] M. Manjaiah, S. Narendranath, S. Basavarajappa, et al., Investigation on material removal rate, surface and subsurface characteristics in wire electro discharge machining of Ti50Ni50-xCux shape memory alloy, Proc. IME : J. Mater. Des. Appl. 232 (2) (2018) 164–177.
[23] S. Narendranath, M. Manjaiah, S. Basavarajappa, et al., Experimental investigations on performance characteristics in wire electro discharge machining of Ti50Ni42.4Cu7.6 shape memory alloy, Proc. IME B: J. Eng. Manufact. 227 (8) (2013) 1180–1187.

[24] V.S. Jatti, Multi-characteristics optimization in EDM of NiTi alloy, NiCu alloy and BeCu alloy using Taguchi's approach and utility concept, Alex. Eng. J. 57 (4) (2018) 2807–2817.
[25] R.J. Beck, D.K. Aspinwall, S.L. Soo, et al., Fatigue performance of surface ground and wire electrical discharge machined TiNi shape memory alloy, Proc. IME B J. Eng. Manufact. (2021), 09544054211028844, https://doi.org/10.1177/09544054211028844. Jul 9.
[26] H. Zhou, W.F. Ding, Z. Li, et al., Predicting the grinding force of titanium matrix composites using the genetic algorithm optimizing back-propagation neural network model, Proc. IME B: J. Eng. Manufact. 233 (4) (2019) 1157–1167.
[27] R. Leese, A. Ivanov, Electrochemical micromachining: review of factors affecting the process applicability in micro-manufacturing, Proc. IME B: J. Eng. Manufact. 232 (2) (2018) 195–207.
[28] R. Chaudhari, J.J. Vora, S.S. Prabu, I.A. Palani, V.K. Patel, D.M. Parikh, Pareto optimization of WEDM process parameters for machining a NiTi shape memory alloy using a combined approach of RSM and heat transfer search algorithm, Adv. Manuf. 9 (1) (2021) 64–80. Mar;.
[29] R. Chaudhari, S. Khanna, J. Vora, V.K. Patel, S. Paneliya, D.Y. Pimenov, K. Giasin, S. Wojciechowski, Experimental investigations and optimization of MWCNTs-mixed WEDM process parameters of nitinol shape memory alloy, J. Mater. Res. Technol. 15 (2021) 2152–2169. Nov 1.
[30] P. Kiran, S. Mohanty, A.K. Das, Surface modification through sustainable micro-EDM process using powder mixed bio-dielectrics, Mater. Manuf. Process. (2021) 1–12, https://doi.org/10.1080/10426914.2021.1967976.
[31] J.B. Valaki, P.P. Rathod, B.C. Khatri, Environmental impact, personnel health and operational safety aspects of electric discharge machining: a review, Proc. IME B: J. Eng. Manufact. 229 (9) (2015) 1481–1491.
[32] N. Sharma, K. Gupta, Wire spark erosion machining of Ni rich NiTi shape memory alloy for bio-medical applications, Procedia Manuf. 35 (2019) 401–406.
[33] A.M.A. Al-Ahmari, M.S. Rasheed, M.K. Mohammed, et al., A Hybrid machining process combining micro-EDM and laser beam machining of nickel–titanium-based shape memory alloy, Mater. Manuf. Process. 13 (3) (2020) 447–455.
[34] C. Prakash, H.K. Kansal, B.S. Pabla, et al., Electric discharge machining–a potential choice for surface modification of metallic implants for orthopedic applications: a review, Proc. IME B: J. Eng. Manufact. 230 (2) (2016) 331–353.
[35] H. Bisaria, P. Shandilya, The machining characteristics and surface integrity of Ni-rich NiTi shape memory alloy using wire electric discharge machining, Proc. IME C: J. Mech. Eng. Sci. 233 (3) (2019) 1068–1078.
[36] H. Bisaria, P. Shandilya, Study on crater depth during material removal in WEDC of Ni-rich nickel–titanium shape memory alloy, J. Braz. Soc. Mech. Sci. Eng. 41 (3) (2019) 157.
[37] M.K. Pradhan, R. Das, Recurrent neural network estimation of material removal rate in electrical discharge machining of AISI D2 tool steel, Proc. IME B: J. Eng. Manufact. 225 (3) (2011) 414–421.
[38] K.S. Naidu, S. Palaniappan, Formation of PANI-PVA salt via H-bonding between PVA and PANI: aqueous coating for electrostatic discharge, sensor and corrosion applications, Sensor. Int. 1 (2020) 100006. Jan 1.
[39] M. Javaid, A. Haleem, R.P. Singh, S. Rab, R. Suman, Exploring impact and features of machine vision for progressive industry 4.0 culture, Sensor. Int. 3 (2022 Jan 1) 100132.
[40] M. Javaid, A. Haleem, R.P. Singh, R. Suman, Significance of Quality 4.0 towards comprehensive enhancement in manufacturing sector, Sensor. Int. 2 (2021 Jan 1) 100109.
[41] M. Javaid, A. Haleem, R.P. Singh, S. Rab, R. Suman, Upgrading the manufacturing sector via applications of industrial internet of things (IIoT), Sensor. Int. 2 (2021 Jan 1) 100129.
[42] K.M. Agarwal, P. Shubham, D. Bhatia, P. Sharma, H. Vaid, R. Vajpeyi, Analyzing the impact of print parameters on dimensional variation of ABS specimens printed using fused deposition modelling (FDM), Sensor. Int. 3 (2022 Jan 1) 100149.
[43] M. Javaid, A. Haleem, R.P. Singh, S. Rab, R. Suman, Exploring impact and features of machine vision for progressive industry 4.0 culture, Sensor. Int. 3 (2022 Jan 1) 100132.
[44] M. Javaid, A. Haleem, R.P. Singh, S. Rab, R. Suman, Exploring the potential of nanosensors: a brief overview, Sensor. Int. 2 (2021 Jan 1) 100130.
[45] M. Javaid, A. Haleem, 3D bioprinting applications for the printing of skin: a brief study, Sensor. Int. 2 (2021 Jan 1) 100123.
[46] M. Javaid, A. Haleem, R.P. Singh, R. Suman, Industrial perspectives of 3D scanning: features, roles and it's analytical applications, Sensor. Int. 2 (2021 Jan 1) 100114.
[47] A. Haleem, M. Javaid, R.P. Singh, R. Suman, S. Rab, Biosensors applications in medical field: a brief review, Sensor. Int. 2 (2021 Jan 1) 100100.
[48] S. Mohapatra, R.K. Kar, P.K. Biswal, S. Bindhani, Approaches of 3D printing in current drug delivery, Sensor. Int. 3 (2022 Jan 1) 100146.
[49] A. Akinola, G. Singh, I. Hashimu, T. Prabhat, U. Nissanov, FSS superstrate antenna for satellite cynosure on IoT to combat COVID-19 pandemic, Sensor. Int. 2 (2021 Jan 1) 100090.
[50] R.V. Rao, P.J. Pawar, Modelling and optimization of process parameters of wire electric discharge machining, Proc. IME B: J. Eng. Manufact. 223 (2010) 1431–1440.
[51] A. Takale, N. Chougule, Optimization of process parameters of wire electro discharge machining for Ti49.4Ni50.6 shape memory alloys using the Taguchi technique, Int. J. Mater. Struct. Integr. 10 (4) (2019) 548–568.
[52] N. Sharma, T. Raj, K.K. Jangra, Parameter optimization and experimental study on wire electrical discharge machining of porous Ni 40 Ti 60 alloy, Proc. IME B: J. Eng. Manufact. 231 (6) (2017) 956–970.
[53] X.P. Dang, Constrained multi-objective optimization of EDM process parameters using kriging model and particle swarm algorithm, Mater. Manuf. Process. 33 (4) (2018) 397–404.
[54] M. Quarto, G. D'Urso, C. Giardini, et al., A comparison between finite element model (FEM) simulation and an integrated artificial neural network (ANN)-Particle swarm optimization (PSO) approach to forecast performances of micro electro discharge machining (Micro-EDM) drilling, Micromachines 12 (6) (2021) 667.
[55] S.H.I. Jaffery, M. Khan, L. Ali, et al., Statistical analysis of process parameters in micromachining of Ti-6Al-4V alloy, Proc. IME B: J. Eng. Manufact. 230 (6) (2016) 1017–1034.
[56] V.P. Srinivasan, P.K. Palani, S. Balamurugan, Experimental investigation on EDM of Si3N4–TiN using grey relational analysis coupled with teaching-learning-based optimization algorithm, Ceram. Int. 47 (13) (2021) 19153–19168.
[57] H. Shahali, M.R.S. Yazdi, A. Mohammadi, et al., Optimization of surface roughness and thickness of white layer in wire electrical discharge machining of DIN 1.4542 stainless steel using micro-genetic algorithm and signal to noise ratio techniques, Proc. IME B: J. Eng. Manufact. 226 (5) (2012) 803–812.
[58] H. Zhou, W.F. Ding, Z. Li, et al., Predicting the grinding force of titanium matrix composites using the genetic algorithm optimizing back-propagation neural network model, Proc. IME B: J. Eng. Manufact. 233 (4) (2019) 1157–1167.
[59] S. Ali, R. Kumar, Hybrid energy efficient network using firefly algorithm, PR-PEGASIS and ADC-ANN in WSN, Sensor. Int. (2021 Dec 21) 100154.
[60] A. Haleem, M. Javaid, R.P. Singh, S. Rab, R. Suman, Hyperautomation for the enhancement of automation in industries, Sensor. Int. 2 (2021 Jan 1) 100124.